Evaluating Performance Testing Procedures for Baseball Catcher's Helmets

Sophia Gervasio, Derek Kruzan, Walter Kwiecinski, Ryan McLaughlin

Advisor: Brian Savilonis

Test Apparatus

Helmet Standards

Head Injury

Table of Contents

Authorship

Sophia Gervasio: Sophia was the primary researcher of the biomechanics portions of the project. She also outlined a suggested viscoelastic model of the collision and assisted with the collection of data from experimentation. She also compared collected data to previous experiments in literature and was also a primary writer for the final report.

Derek Kruzan: Derek assisted Sophia with producing the Biomechanical Viscoelastic models. He also aided Walter and Ryan in the design and assembly of the mechanical and electrical components of the system, and assisted with the collection of data. He served as a primary writer for the report.

Walter Kwiecinski: Walter was the primary designer of the mechanical components of the system. He assisted with the calibration of the system and with the collection of data. He served as a primary writer for the report.

Ryan McLaughlin: Ryan was the primary designer of the electrical and power transmission system for the test apparatus and assisted in the system's assembly. He assisted with the calibration and the collection of data. He served as a primary writer for the report.

Acknowledgments

The team would like to extend its deepest gratitude to the following individuals for dedicating their time and resources to help advance the goals of this project. Each individual contributed greatly in guiding us to the completion of this project:

- Brian Savilonis
- Kenneth Stafford
- Barbara Fuhrman
- James Loiselle
- Thomas Kouttron

Abstract

Collisions between a baseball bat and a catcher's helmet is a rare, yet severe impact that often leads to head and brain injuries. Catcher's helmets are currently designed to pass NOCSAE standards in a linear drop test. A testing apparatus that replicates a batter's backswing was prototyped to incorporate angular acceleration and tested by colliding a baseball bat into a headform. Testing was performed at six velocities between 11 and 25 mph with and without helmet protection. Peak G and Severity Index were measured at the headform's center of mass to demonstrate collision effects at the brain. Collected data validated existing drop test for 1D testing, but suggests NOCSAE standards may test unrealistically high energy impacts. Risk of injury decreased significantly when a helmet covered the headform and is explained through a viscoelastic model. Future modifications in helmet designs and testing procedures will likely incorporate angular acceleration to improve the three-dimensional reaction models of the brain.

Table of Figures

Table of Tables

Chapter 1: Introduction

There is a growing awareness and heightened interest in brain-related injuries in major league sports. With better understanding of these injuries, Major League Baseball (MLB) has taken steps to mitigate head injuries to their players through new non-collision policies and improved safety equipment. One cause of injury that has not been substantially investigated is backswing collisions between baseball bats and catcher's helmets. Improvements to current catcher's helmets are being researched, but current testing and research is limited to helmet "drop tests", which attempt to model the physics of this collision. Although this test is repeatable, there is question as to whether or not testing mechanisms for these helmets should accurately represent bat-helmet impact force, speed, and impact area to appropriately estimate helmet, bat, head, and neck reactions from this type of collision.

The goal of this project is to develop an improved test system that will repeatedly and accurately replicate the collision between a baseball catcher's helmet and a batter's backswing. Data collected from this collision will be used to compare the developed testing mechanism with current testing methods to determine any weaknesses in current helmet designs. Finally, this project will identify the severity of impact on biological components, such as the skull and brain, as a result of this collision.

Chapter 2: Literature Review

2.1 Injuries to Baseball Catchers

The inherent risk that catchers face during every pitch during a baseball game has influenced the protective gear which they wear. Baseball players face one of the highest rates of ball-contact injuries among all of sports (Fraser 2017). A study from 2010 to 2012 showed that, even though catchers only account for 11% of the players on a baseball field, they accounted for approximately 40-50% of concussions in professional baseball (Boden 2004). Most catcher injuries are caused by ball impacts as the average MLB pitch speed is about 92 mph, and maximum speeds regularly reaching over 100 mph.

Another main type of collision that has caused severe injuries to catchers is from bats during a batter's backswing. Similar to impacts from batted balls, these impacts have a low occurrence but pose a high risk of severe injury. Unlike potential risks due to ball impacts, there have been minimal actions taken to help reduce bat collisions. One action trying to reduce these injuries is increased helmet testing standards.

2.2 Existing Test Mechanisms

The National Operating Committee on Standards for Athletic Equipment (NOCSAE), is the governing body which creates standards for catchers masks. Most catcher equipment companies not only test to abide by NOCSAE standards; they test their products to withstand several specific situations not represented within NOCSAE test scenarios (NOCSAE 2018). One of these scenarios is an inadvertent collision between the catcher and a baseball or softball bat on the back-end of a batter's swing. This situation, while rare, can result in a serious head injury for the catcher. This test attempts to simulate the momentum conservation of the system by dropping a helmet and head fixture from a certain height onto a bat-shaped anvil. The test drops the helmet and head assembly from a particular height to achieve the same linear momentum as a bat during a swing.

While this drop test does seem to accurately model the momentum of the bat and helmet system, several other important dynamic elements of the collision are not accurately represented in the test. In the real scenario, the helmet and head are stationary while the bat is in motion; the drop test reverses the motion roles of the objects in the system. The coefficient of restitution, represented by Equation 1, is also not accurately modeled by the drop test. In this case the acceleration experienced by the headform may be different in the test that what is experienced in reality, which may change the likelihood of resulting injury. Modeling the coefficient of restitution between the two rigid bodies would be necessary for simulating the effects of the impact following the immediate collision.

$$C_r = (V_{fb} - V_{fa}) \div (V_{ia} - V_{ib}) \qquad \text{Eq. 1}$$

When considering the design of helmets, each of these variables could have an effect on the type of liner selected for for catcher's helmets. While current test standards reflect a low velocity impact of about 10 mph, collisions between a bat and catchers helmets exceed velocities of 20 mph or greater, which may have and impact on foam performance. Data on the speed of back swings for baseball players is not readily available, so the team had to collect data. To do so the team measured the bat speed of a member of the WPI men's baseball team. An analysis on bat speed was done using a slow motion camera and two video analysis softwares, Motion Pro (shown in Figure 1) and SkillSpector. Both softwares indicated back swing speeds (at the tip of the bat) at the point of collision with a catchers mask is about 22 mph. Speed values captured at the front half of the swing matched expected values based on available published data, indicating that the backswing speeds measured were reasonably accurate.

Figure 1. Bat Path and Velocity Tracking screen capture from MotionPro software

2.3 Catcher Helmet Structure

Protective headgear in sports was not popularized until the late 1800's, with the emergence of American football and resulting injuries such as skull fracture and death. Leather helmets were developed in response to these injuries, and since then protective headgear in sports has continually evolved (Hoshizaki 2004). While most sports feature their own unique helmet designs, common characteristics of helmets exist across sports. Many of today's helmets feature a hard exterior layer or shell and a soft liner. Most commonly, the outer material is made of an ABS shell with an inner vinyl nitrile padding. The soft lining in current helmets are responsible for energy attenuation during impacts as they are compressed. Materials that are more stiff are more effective at absorbing energy for high speed impacts, but less effective at absorbing low speed impacts that could still result in injury. Vice versa, less stiff materials are more effective at absorbing energy during low speed impacts and are less effective during high speed impacts.

Voigt Modeling of Helmets

In one source, a finite element analysis (FEA) in ABAQUS software with a simplified batting helmet model on a head including four layers of analysis: outer helmet shell, inner shell (foam lining), cortical skull bone, and cerebral spinal fluid (CSF) (Gholampour 2017). The model suggested is outlined in Figure 2 with the skull and shell represented as a spring and the foam and CSF as dampers. FEA results showed that the outer shell layer experiences about 70 times more stress than the inner foam layer. The impact shows both the dispersion of stress on the outer shell as well as localized stress on the foam. The author also comments that when they doubled the foam layer and results increased in both deformation and stress concentration compared to the single layer.

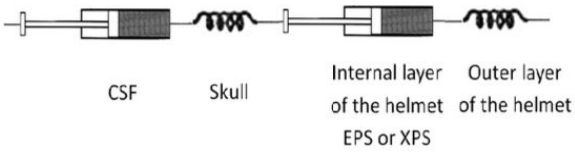

Figure 2. Suggested viscoelastic model of head wearing a helmet

"Skull Cap" and "Hockey-Style" Helmets

The two main styles of helmets for catchers are the "hockey-style" helmet and the "skull cap", as seen in Figure 3. The skull cap style helmet is the older, traditional style of catcher's' headgear, but in recent years the hockey style helmet has grown in popularity due to its increased protection. However, while many players have switched to the hockey style mask, many still use the skull cap since it is easily removable during play. For this reason, approximately two-thirds of MLB players wear the skull cap over the hockey style helmet (Barksdale 2015).

(a)

(b)

Figure 3: Examples of a (a) skull cap and a (b) hockey-style helmet

2.4 Industry Standards

The National Operating Committee on Standards for Athletic Equipment (NOCSAE) is the governing body which certifies the safety of protective sporting equipment and ensures that they adequately protect players from injury. All catcher's masks must pass several tests before being approved by these standards for use from Little League to MLB under standard ND024. The standard outlines two main procedures in which seven helmets of the same model must be tested to achieve certification. The first test involves firing softballs at 55 mph to impact the front and sides of the helmet. This ensures that the helmet would protect against impact from a batted ball during a game. The second test is a drop test used to simulate the impact of a bat on the side

and back of the catcher's mask. The head is dropped onto an anvil with a semi-circle protrusion which is approximately the diameter of a baseball bat (2.5 inches). The helmet is tested so that it achieves a final impact velocity of 4.23 m/s (19.16 Newton * seconds momentum) in four different locations: right, right rear boss, rear, and a random location. Figure 4 visualizes the orientations of the helmet during these drop tests.

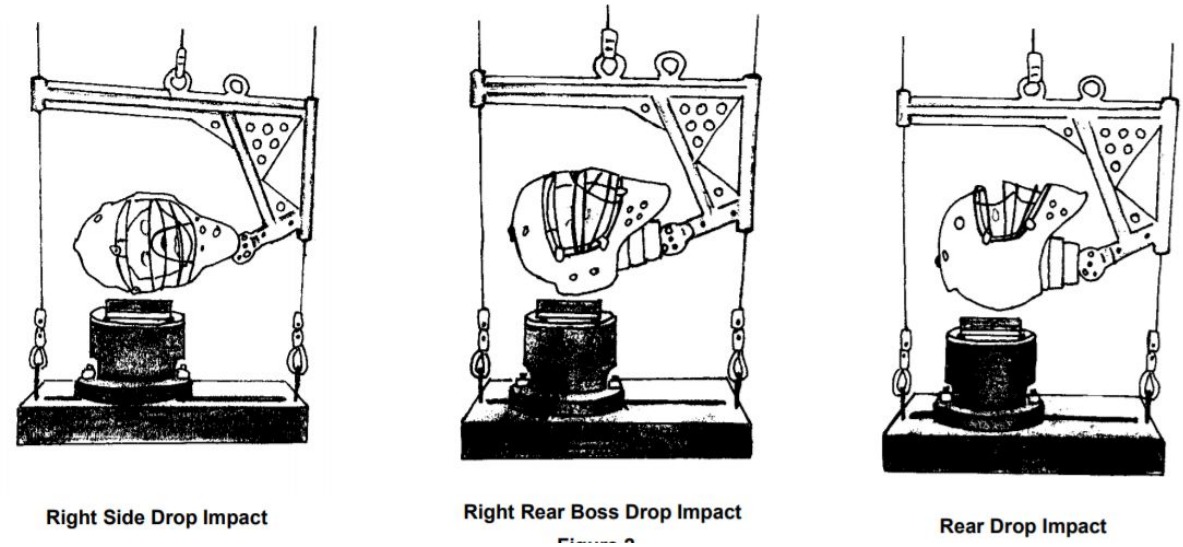

Figure 4: Drop test locations for NOCSAE helmet standards (NOCSAE 2018)

All tests for baseball catcher's helmets are measured by a performance metric called the Severity Index. The Severity Index is a function of the acceleration of the head from experiences in the x-direction, y-direction, and z-direction. To meet the standard, the head must experience a Severity Index under 1200 SI for each test performed. This number was chosen as the accepted threshold to avoid severe head injury (NOCSAE 2018). The team's tests will measure Severity Index with the new test apparatus so that this data can be compared to current industry standards and tests.

2.5 Injury from Collisions

Concussions

Concussions are caused by trauma to the brain and central nervous system. The brain is made of soft, fatty tissue with a viscoelastic liquid consistency and is protected by the skull and surrounding tissues, it can internally be mobile during impact and result in stretching, bumping, penetration, and tearing of brain tissue. Concussions can therefore be a direct cause of a variety of symptoms from headaches, blurred vision, and memory loss to sleep deprivation, anxiety, and depression (Robbins 2017). Concussions can have an extreme impact on one's brain tissue and function and, therefore, the physiological growth and development of those who have experienced of concussions (Banac 2011). The implications of concussive collisions can be so

detrimental that new standard procedures for those who experience athletic head collisions are being put in place to ensure safety in all sports settings.

Bone Composition and Fractures

The two different types of bone are cortical (compact) bone and cancellous (trabecular) bone. Cortical bone is a hard, exterior layer of bone that is dense in composition whereas cancellous bone contains an open cell network of porous bone and is the internal composition with a lower density and weaker mechanical properties. Cortical bone has a much higher elastic modulus than cancellous bone and can disperse the energy of impact in a collision. This compares to cancellous bone that, because of its increases surface area and porous network, is able to absorb shock energy in a collision. The skull's composition is outlined in Figure 5 with compact bone on both sides of the cancellous bone.

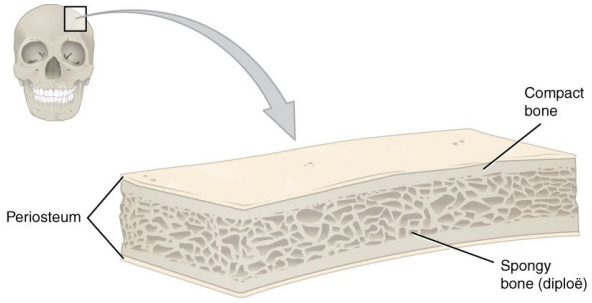

Figure 5. Cross-sectional image of skull bone composition (OpenStax).

High impact collisions on human bone can lead to bone deformation and bone fracture. Human bone is a viscoelastic material and experiences elastic and plastic deformation under applied stress. In plastic deformation, the viscoelastic bone is unable to return to its original shape and loses some of its mechanical properties. If load continues to increase, the ultimate tensile strength of the bone can be reached until the bone experiences failure and is fractured.

Head Injury Predictions

Testing mechanisms often determine helmet performance by measuring Severity Index, as required by NOCSAE standards. This accounts for the acceleration effects experienced at the brain after an impact and calculated by Equation 2.

$$\mathrm{SI} = \int_0^{t_1} \mathrm{a(t)}^{2.5}\, dt \qquad \text{Eq. 2}$$

Although tests were performed using angular acceleration, the team compared the collected data to literature using linear acceleration due to availability of current research and understandings. The team started with the Wayne State Tolerance Curve to understand the relationship between acceleration, impact duration, and injury severity. This curve is explained

in Figure 6 as a smaller time duration and lower acceleration combination is likely to decrease risk of severe head injury (Namjoshi 2013).

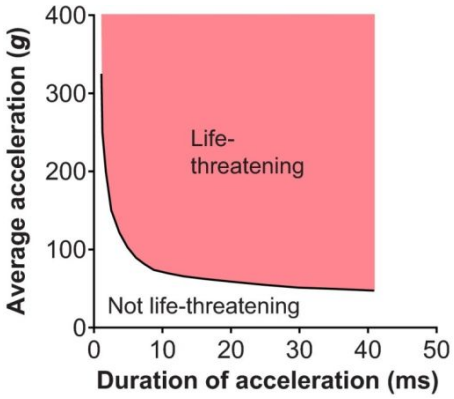

Figure 6. Wayne State Tolerance Curve

Another way head injury risks are predicted is by using calculated Head Injury Criterion (HIC) values. Using this, there are many limitations such as a lack of consideration for injury type, rotation, mass, or direction. However, it is better than only using acceleration to calculate the risk as HIC does include the importance of impact time duration and acknowledges the importance of prior research (Newman, 2005). This value can be calculated using Equation 3.

$$HIC^* = (t_2 - t_1)\left[\frac{1}{t_2 - t_1}\int_{t_1}^{t_2} a(t)dt\right]^{5/2}$$

Eq. 3

Chapter 3: Project Strategy

3.1 Initial Client Statement

Design a testing apparatus which more accurately simulates the physics of a collision between the backswing of a baseball bat and a catcher's mask.

3.2 Objectives and Constraints

Develop and utilize a test system to better understand the inadvertent contact of and potential injuries resulting from baseball bat and catcher's helmet impact.

1. Develop a test apparatus that accurately simulates contact between a bat during the backswing of a baseball player and a catcher's helmet.
2. Use collected data to compare the drop test with the test mechanism developed.
3. Identify any weaknesses in current helmet designs and possibly develop recommendations to improve future helmet design.

4. Use collected data to analyze risk of injury.

Using the measured bat speed of a batter's backswing discussed in section 2.2, key values were calculated that defined the parameters of the test system. Using a 32", 32 oz. model bat and the measured speed of 22 mph, necessary values including torque, rpm, and spring constant needed over an assumed 270 ° acceleration distance. Table 1 shows these values.

Table 1. Key Values For Test Apparatus

Given :		
mass:	0.91	kg
Length:	0.81	m
v:	9.8	m/s
I:	0.20	kgm^2

Calculations		
Property	Value	Unit
Angular Velocity (ω)	12.09	rad/s
Revolutions per minute (rpm)	115.4	-
Angular Acceleration (α)	15.51	rad/s^2
Torque (τ)	3.099	Nm
Torque (τ)	27.43	in-lb
Power	0.03742	kW
Power	0.05016	hp
impact Force	2721	N

3.3 Revised Client Statement

The client wants a testing apparatus which simulates a baseball batter swing with a horizontal bat path, reaching 30 mph and resulting in a collision with a catcher's mask. The device should be useable in lab space, safe, easy to use and and repeatable.

3.4 Project Approach

The team researched all aspects of catcher's helmets including testing methods, material selection, current standards, manufacturing companies, and structure. Aspects directly related to helmet impacts, including concussion and fracture risk, were also researched to prepare for biomechanical analyses. The team then defined system criteria and needs for a testing apparatus and brainstormed possible test apparatuses to construct to fulfill test needs. Various conceptual designs were explored with calculations and feasibility testing. The team then seeked professional feedback and modified optimal designs until a final test design was chosen.

Chapter 4: Design Process

4.1 Needs Analysis

The team focused on developing a repeatable and accurate replication of the collision between a baseball bat and catcher's helmet. To address this, a design matrix was developed with various weighted criteria for each potential system. The criteria are outlined in Table 2.

Table 2. Test Apparatus Criteria

Criteria	Description
Velocity and Energy of Backswing	Replicating a back-swing as accurately as possible is key to this system. The velocity needed at the point of impact is a minimum of 30 mph, according to our bat speed analysis shown in section 2.2.
Horizontal Bat Path	Ideally the system should have a horizontal bat path so that it best replicates the back swing of a baseball player. This will ensure that test helmet can be correctly oriented and that gravity will not have unrealistic effect on the simulated neck that is supporting the helmet and headform.
Size	Test system size is restricted to available lab space. The system will be indoors, with both height and safe operating space as factors in the system's size.
Safety	The system a bat moving at high velocity, which introduces safety risks. Important factors being considered include making sure that the user does not need to enter the bat path of the system and is also safe from potential debris resulting from the collision. The ability to start and stop the system will be in a controlled and safe manner.
Risk of Bat Breaking	If the system will use a wooden bat there is a risk of breaking the bat as it accelerates. Increased acceleration results in increased torque. The bat will need adequate distance to accelerate to avoid this.
Cost and Sustainability	The cost of the system will vary depending on the chosen power element and the equipment available to the end-user of the system. The system would ideally be designed for long-term use with minimal cost for upkeep. The team has a budget of $1,000 for the construction of the test apparatus.
Ease of Use and Repeatability	Ease of use is an important design parameter for the system. Our system is being developed for Research and Development at a baseball equipment manufacturer. Therefore, it is critical that future operators of the system can quickly learn how to properly and safely use the system. It is expected that the system will be durable enough to withstand repeated use with limited variability in performance to allow for accuracy and repeatability.
Ease of Future Modifications	While the current system will address the need for a test system that more accurately models a bat to helmet collision on a horizontal swing plane, the system will be easily modified for future improvements.

4.2 Conceptual Designs

Motor

The first conceptual system design uses a bat-swinging system driven by a DC motor. From calculations outlined in Table 4, the motor would have to move the bat at 115 rpm with a torque of 3.1 N-m. Small motors are capable of providing the power necessary to reach these values, however use of a motor would likely require the complementary use of a gearbox to supply the appropriate torque and shaft rpm for the system. Gearboxes are capable of translating fast motor rotation with little torque to slow rotation with high torque, which would be necessary for our system. Electrical instrumentation would be crucial for controlling the voltage and current sent into the motor and the start/stop of a bat-swing system cycle.

Compressed Air

The use of compressed air could be extremely beneficial in this type of test mechanism as built-up air pressure can be released at once to force the bat to move with a significant angular acceleration. This design can be incorporated into a horizontal bat path with a model of feasible size and cost. Sustainability of the machine would depend on the end-user's ability to supply and control an appropriate amount of air at a required pressure of approximately 80 psi. This mechanism will also be kept in mind as an option to supplement other possible testing designs (i.e. compressed air and pendulum) to enhance design measures and use the most efficient method of impact. An air system could potentially be powered by shop air, but even without shop air compressed tanks could be used to power the system.

Pendulum

A pendulum model uses gravity to create momentum of an arm that would then accelerate until it strikes the helmet. Given average bat swing speeds, estimated height and mass of an arm in a model are predicted in Table 3 in order to replicate the speed and energy at which a bat would collide with a helmet in a game. Optimal values taken from this calculation would result in a test apparatus 1.5 meters high and about 30 kg in mass.

Table 3: Mechanical Values of a Potential Pendulum Model

Velocity (mph)	70.0
Upper velocity (m/s)	31.3
KE (Joules)	444

Height (m)	Mass (kg) - upper
0.5	90.52
1	45.26
1.5	30.17
2	22.63

This pendulum model does not directly replicate a horizontal bat path, but could be modified to promote a horizontal bat path. As noted in Table 3, the design is able to be modified to reach the velocity and momentum of a backswing, but drawbacks of this include increased size and decreased safety. Since the pendulum design for the system relies on gravity as its source of energy, it will not need a power source. However, the pendulum design would require a larger and more complex frame, warranting higher frame cost compared to the frames of the motor, compressed air, and torsional spring frames.

Torsional Spring

A torsional spring system could be one of the least expensive systems in the proposed models. The system would work by loading the spring over the proposed distance using a spring that would supply the necessary energy as outlined in Table 3. However the spring system offers several drawbacks as well. The first of which is the fact that the system would reach the upper limit of standard torsional spring coefficients at a final speed of 22 mph. An additional complication is the fact that torsional springs work on a fixed diameter, meaning whichever shaft our design implemented would have to match the diameter of a torsional spring. An additional mechanism for loading the spring would have to be considered, since manual loading of the spring could be dangerous to the user if they were directly in the path of the bath.

4.3 Alternative Designs

Bat Fixture and Base

Basic design components include a bat fixture, a shaft, a bearing, and a base. A universal base that can be used for all potential designs outlined in previous sections is desired to promote ease of modification for future iterations. Figures 7a and 7b include CAD models of potential universal base ideas. This design uses a wooden base with three legs for stability. The team determined enclosing the bat path may be unnecessary if the bat path includes clearly marked restricted areas with suggested personal protective equipment for users.

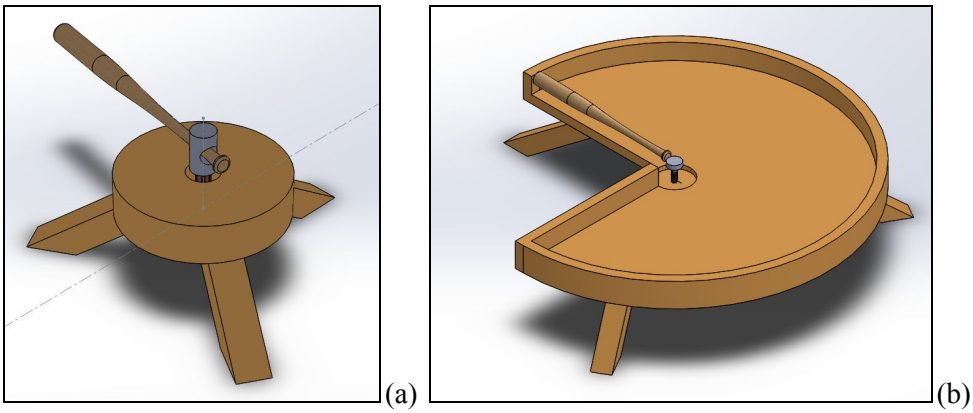

(a) (b)

Figure 7. (a) First and (b) second designs as a CAD Drawing

A goal for the test apparatus is to ensure that the shaft can rotate freely with minimal friction. The use of ball bearings are included in the design to avoid friction and remove uneven loading caused by the moment arm. Figure 8 shows a potential design of how the ball bearing would attach to the shaft.

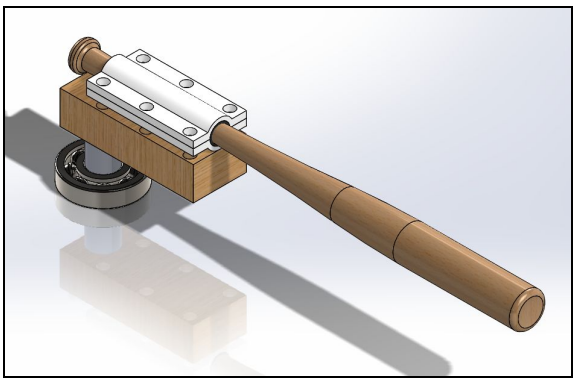

Figure 8. Ball Bearing Incorporated into Shaft for Horizontal Movement

As mentioned above, the base of the test apparatus will be universal for all design concepts. The team first brainstormed the idea of the rectangular prism which is modeled in Figure 9. In actuality, the base will be open to allow for design components, such as the motor, to be easily accessible to the operator and release heat from the system without affecting itself. The team foresees future designs incorporating this rectangular base, with the addition of four legs attached below it, and a platform for the shaft and bat fixture above it. This design will be just as structurally sound as the design in Figure 9 with decreased weight, material and cost.

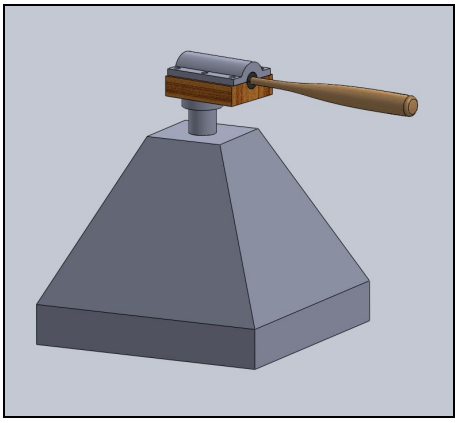

Figure 9. Tapered Base Prism Design

A clamp connected the the drive shaft that consists of two pieces bolted together around the bat handle will be used to fix the bat into place. This enclosure will be fixed into a wooden block attached to the shaft of the device. The clamp will also incorporate an inner foam lining that will form to the bat's tapered shape to hold it in place in the clamped enclosure. Figure 10

shows initial CAD models of these designs as Figure 10a utilizes two clamps and Figure 10b uses the wooden block attached to the shaft as the lower half of the clamp.

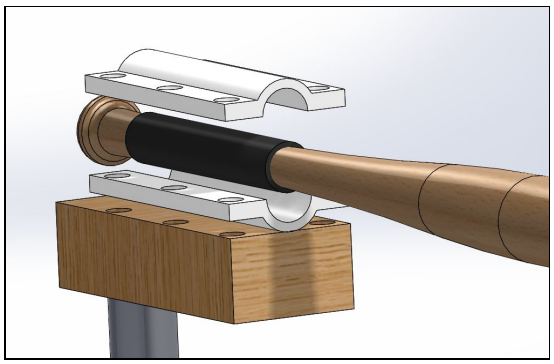
(a)
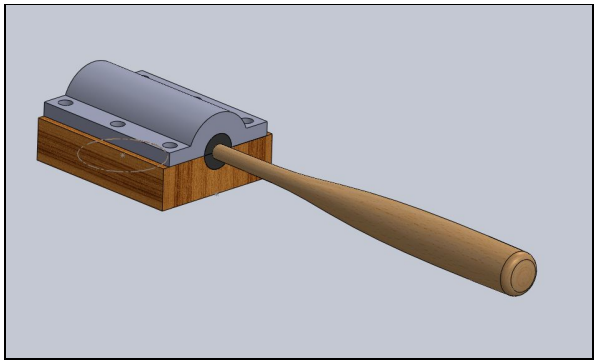
(b)

Figure 10. (a) First and (b) second clamp model CAD drawing to hold bat

4.4 Final Design Selection

Decision Matrix

After compiling the 4 different design concepts, the team utilized a Decision Matrix to determine which design best fit their design criteria. Each design iteration was weighted on a scale from 1-3, with 1 being an optimal design and 3 being sub optimal. After rating how each design fit the design criteria, the totals were added up and compared. The design with the lowest score was the motor design and thus was deemed to be the most optimal design to prototype and test. Table 4 depicts the decision matrix used to select the Motor Design.

Table 4. Decision Matrix of Design Options

Test Apparatus Decision Matrix					
1=Yes, 2= Can be fixed, 3= No					
Parameters	**Motor**	**Air**	**Pendulum**	**Spring**	**Weight**
Horizontal Bat Path	1	1	2	1	2
Meet velocity of backswing	1	2	2	2	
Meet Energy required of backswing	1	3	2	1	2
Ease of Future Modifications	2	2	2	3	
Size	1	1	3	1	
Safety	2	2	2	3	2
Risk of Bat Breaking	2	2	2	2	
Construction Cost	2	1	1	1	
Long-term cost/ sustainability	2	1	1	2	
Ease of use	3	1	1	2	
Total	**21**	**22**	**24**	**23**	

System Summary

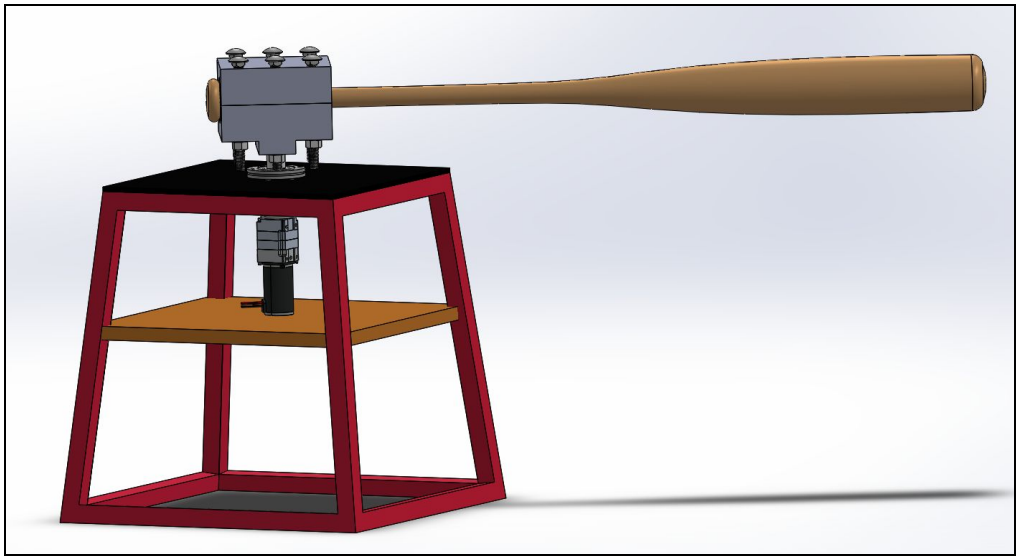

Figure 11. Motor-Powered Test Apparatus

Figure 11 shows the design of the selected system. The base of the system was a purchased 18-inch plyometric box. While initial designs included similarly-styled bases manufactured by the team, the purchased box allowed for a much more robust and sturdy design than the team could have achieved with a homemade base. Manufacturing of the base was limited to modifying the box with a hole for shaft placement through the top of the base. The motor was fixed on a wooden platform along the axis of the shaft. The integration of all other components is discussed below.

Motor and Gearbox

The motor-based system was determined to be the most viable solution for powering and controlling the test apparatus. Key reasons for selecting a motor were increased control and repeatability of the required 30 mph speed. Additionally, the 95 Watts required to accelerate the system over 270° of rotation was most easily generated by a motor compared to the other power sources considered. A CIM motor with the performance curve shown in Figure 12 was selected. The circuit for powering the motor is described later in this paper in the Circuit Design subsection. Using these performance metrics as well as the known required outputs for our test system, the team determined that this motor would suffice with a gear reduction of about 18:1, as shown in Table 5.

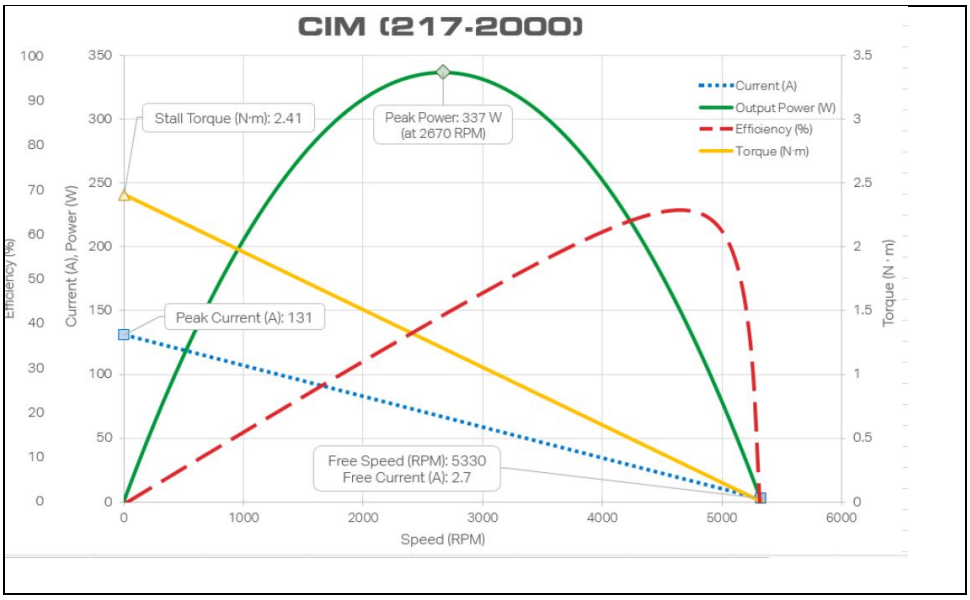

Figure 12: Motor performance curve (Vex Robotics)

A two stage planetary gearbox with a 16:1 reduction ratio was selected due to a lack of availability of 18:1 gearboxes, and a lower ratio as opposed to a higher was selected to allow for higher speeds. The team calculated that a 16:1 ratio would work as long as the motor RPM and torque were modified to accommodate the ratio change to reach the required output RPM/torque. The planetary gearbox system was selected because of its compact structure, ease of assembly, and modularity by using different planetary spur gears. Modularity was a significant factor as components may be needed to be replaced to alter the gear ratio or the output shaft for interfacing with the rest of the system. Another gear reduction system considered was a chain drive, which has the ability to change the gear ratio by replacing its sprockets. However, due to the concerns of maintaining chain tension, the team elected to use a gearbox. Table 5 depicts the calculations used to determine the optimal gear ratio for the system.

Table 5: Final Gearbox Calculations based on 30 mph bat swing

	RPM	Torque (in lbs)	Current (A)
Needed output	157.4	50.98	N/A
Motor output	2832	10.00	63.50
Gear ratio needed	17.99		

Shaft and bearing

The round 0.5-inch diameter gearbox output steel shaft inserts directly into the test apparatus drive shaft shown in Figure 13. This material was chosen for both its strength and the favorable friction properties associated with aluminum and steel contact between the gearbox output and the shaft. This ultimately lead to a higher safety factor for failure for our shaft. The size of the shaft was selected based on a stress analysis conducted in MathCAD. This analysis

yielded a safety factor of 4.9. This safety factor was calculated for the estimated impact load from the collision with the helmet. A key assumption in this calculation was that the drive shaft absorbs all of the impact energy. As a result, the safety factor is likely even higher than the value calculated, because energy will likely be dispersed among other components. The gearbox shaft will be faced as shown in Figure 13 to allow for a more effective transfer of torque to the bat clamp.

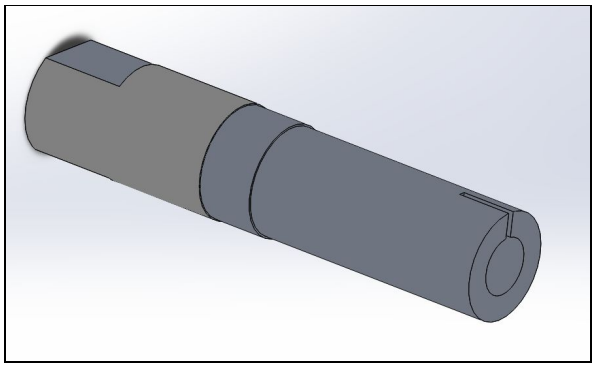

Figure 13: CAD drawing of Faced Shaft

To connect the shaft to the bearing, the outer diameter of the shaft had to be machined to 25mm. A stepped shaft design allows the bearing to be press fit onto the shaft as shown in figure 14.

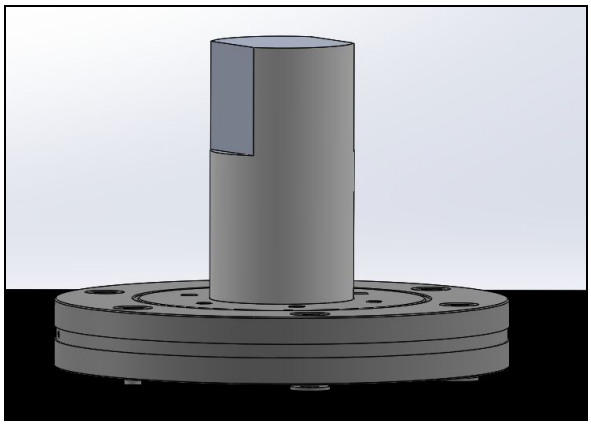

Figure 14: CAD drawing close up of shaft and bearing

Initial designs include a key and keyway to secure the drive shaft and gearbox output shaft together, but due to limitations in machining, this was not possible. The final design includes a drive shaft that is slotted and the clamping collar shown in Figure 15 will be used to tighten the drive shaft around the gearbox output shaft. This design prevents backdrive on the gearbox and motor by allowing the gearbox output shaft to slip relative to the drive shaft when it is subjected to excessive torque. The location of the shaft collar can be seen in Figure 16.

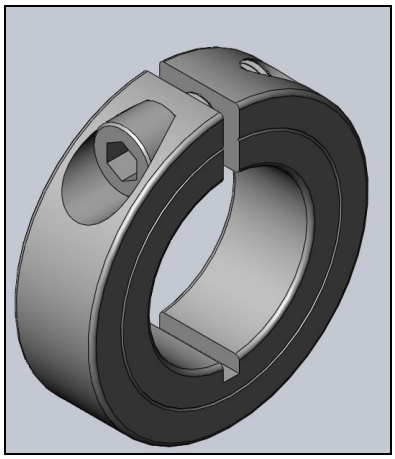

Figure 15. Drive Shaft Clamping Collar

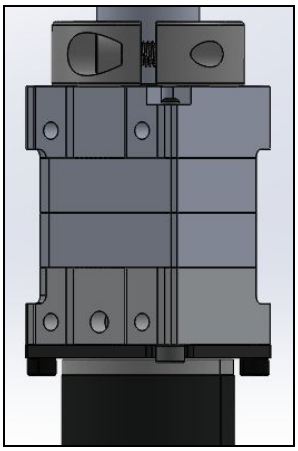

Figure 16. Motor Gearbox, Collar, and Shaft Assembly

Bat Clamp

Requirements of the bat clamp include the need to withstand the loads experienced during impact, the ability to firmly hold the bat despite a tapered handle, and ease of manufacturability. Preliminary designs consisted of a top and bottom half made of machined metal parts or wood, and a foam material that lines the cut out for the bat. A foam was implemented so that the clamp could form to the shape of a bat handle when the clamp is tightened. While metal and wood were preliminary choices due to their strengths, machining would have been difficult to complete.

With these factors in mind, the team opted to develop a 3D printed clamp that could be developed more easily, quickly, and inexpensively. Figure 17 shows the current design, still composed of two halves and a foam liner, but made of 3D printed PLA. These two halves are secured together with steel bolts. The bottom half of the clamp is press fit onto the faced end of the drive shaft.

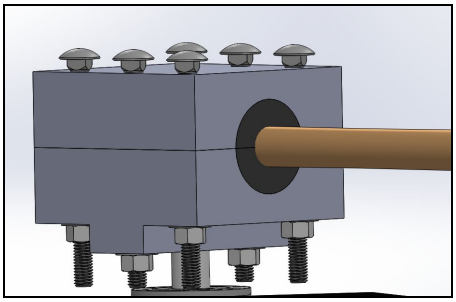

Figure 17: CAD drawing of selected clamp design

The components were designed to be larger than the metal and wood iterations so that there is more material to absorb impact energy. An adequate material volume was calculated by calculating the area under the stress strain curve of PLA (J/m^3) and dividing the impact energy (J) by this value. Theoretical stress calculations then showed that the material and design should withstand the loads and from the bat and helmet collision at its weakest point shown in Figure 18. This is despite the much lower yield strength of 3D printed materials compared to machined metals. This was done using an approximated force of impact calculated by estimating the duration of impact and calculating the impulse as shown in Equation 4.

$$F = m \times \Delta v / \Delta t \qquad \text{Eq.4}$$

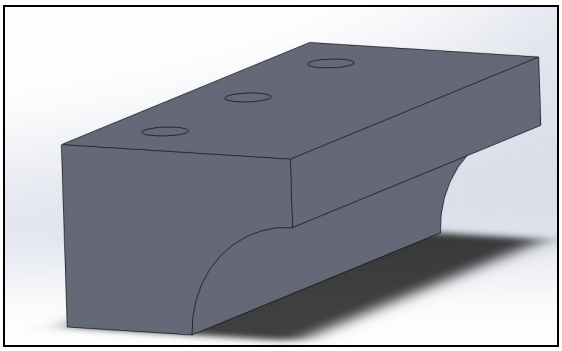

Figure 18: CAD drawing of Cross sectional area where stress was measured

For the stress calculations it was assumed that all of the energy from the impact is experienced by the bat and clamp as opposed to the helmet, and that just one half of the clamp would experience all loads. This force was then applied over the cross sectional area shown in Figure 18. This resulted in a stress of approximately 0.47 MPa. PLA's average yield strength is 36.3 MPa, but given the 30% in-fill rate of the 3D print this value is closer approximated by 12.1 MPa for this component. This allows for a safety factor of about 25 for clamp. The team was unsure of the actual yield strength of the PLA due to the non-homogenous nature of 3D printed materials. Therefore, the higher safety factor value serves to compensate for these potentially significant unknowns.

Circuit Design

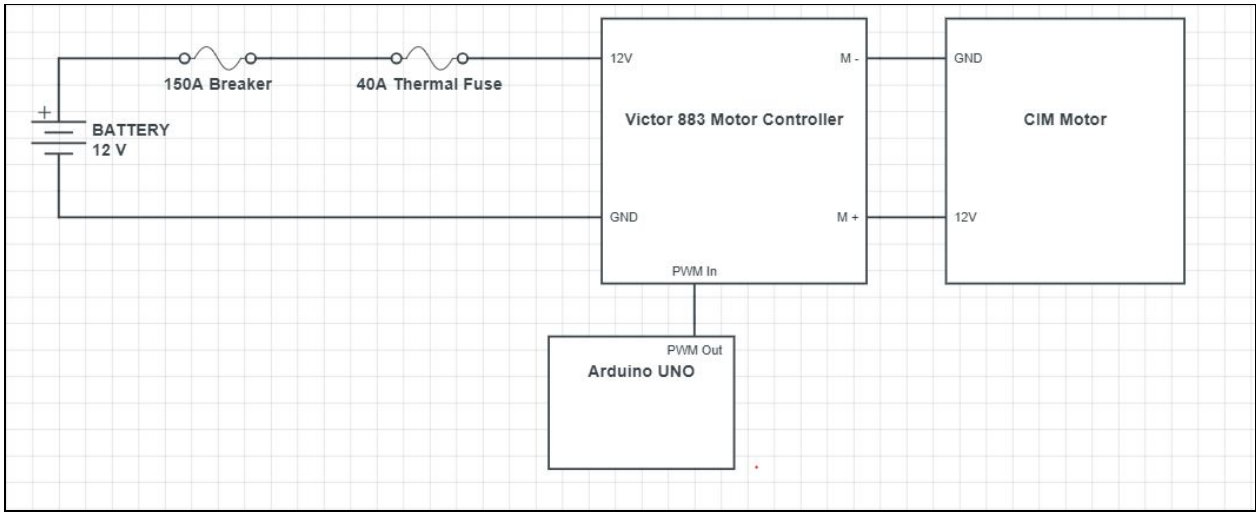

Figure 19: Circuit Schematic

The circuit schematic shown in Figure 19 was designed to safely power and accurately control the movement of the system's shaft. This section details the components chosen, the rationale used for their selection, their functions, and any pertinent properties.

Motor

The intricacies of a motor's performance and its technical demands make it the most important component of the power system. Due to this, the circuit layout and its components were selected based upon the particular requirements of the chosen motor. After several consultations with professors and colleagues experienced with motors, the team chose to use a CIM motor. This motor is commonly used in robotics and is easily adaptable to a variety of system needs. The CIM motor can deliver nearly 340W of power, which is more than triple the power demand from the system (~ 94W).

Current draw was the largest issue presented by the use of the CIM motor. Referencing the CIM motor performance curve shown in Figure 12, the CIM motor draws approximately 70 amps at the required power. This is a high amount of current which needed to be accommodated safely with components rated for such amperage. While the motor will draw a high current, a single test cycle only draws from the power source for approximately half of a second. This cycle time is very low, which helps to minimize the electrical risk posed by the system despite the high expected current.

Battery

Standard AC wall outlets would not suffice as viable sources of current since they typically can only provide approximately 20A. The team selected a 12V, 8Ah sealed lead-acid

battery was chosen as the power source, allowing the system to draw the current it needs instantaneously. The selected battery with a high capacity of 8Ah is more than sufficient for the many test iterations needed for this project.

Circuit Breaker/Switch

Discussions with robotics colleagues and professors helped the team understand that a "master switch" would be necessary for the system to be able to cut power to the circuit. A 150A switch circuit breaker was chosen for its ability to act as both a circuit protection element and as a safety switch. This switch cuts power once 150A is reached or once the switch is activated by the user. This switch was located away from the mechanism for safety and ease of use for the operator.

Fuse

It was recommended that the circuit includes a fuse between the breaker switch and the motor controller to further protect the system. A 40A thermal ATC style fuse was selected to add an additional layer of circuit protection. Thermal fuses cut power once a threshold level of heat accumulated over a period of time activates the fuse. These fuses are designed to withstand a time delay (over 2 seconds) before cutting power and cutting the circuit, allowing for our system's test duration of less than half a second to operate above the rated current of the fuse.

Motor Controller and Microcontroller (Arduino)

A Victor 883 motor controller was used to control the operation of the CIM motor. This controller receives a 12V input and allows for multiple settings of current flow into the motor. This motor controller has both brake and coast configurations in addition to forward and reverse drive settings. The brake setting is used to halt a motor, whereas the coast setting is used to allow the motor shaft to continue rotating once the drive signal has ceased. Since the system replicates a batter's backswing, the coast configuration is ideal for the design. The motor controller receives specific digital PWM (pulse-width-modulation) drive signals from a microcontroller and displays these signals via a colored LED.

The team selected an Arduino UNO microcontroller to write and send signals to the motor apparatus. An Arduino code script has been developed to send a drive signal (in microseconds from 1000 to 2000) to the motor for a specific duration of time (in milliseconds). Once properly calibrated, the motor controller allows for repeatable and controlled function of the motor.

Wiring and Connectors

From the CIM motor data sheet, the team noted that the motor wire is AWG #14. From research, AWG #14 wire may not be suitable for handling amperage as high as 70A. To safely accommodate for these high currents, the team chose to use a higher-rated wire of AWG #10

throughout our system. Components were connected by either ring terminals or Anderson PowerPole connectors.

Additional Safety Information

The team understands that this apparatus could be dangerous if not operated correctly. The system draws a large amount of current to supply the power to our motor which could also be dangerous. Several robotics and electrical specialists were consulted to ensure that the machine is connected safely and correctly.

The system was designed so that the user has the ability to operate the system from a distance of 12 ft away, limited by the USB cable length between the Arduino and operating computer. The master switch was also wired to be within direct reach of the operator. This ensures that the operator is a safe distance away from the bat swing while being able to control the circuit and Arduino. Our team plans to implement a "restricted entry" radius which would prevent individuals from standing too close to the test apparatus. Finally, the team placed barriers around the test apparatus to ensure that the operator and observing individuals are protected from flying debris that may result from a test cycle.

The final model was constructed as shown in Figure 20.

Figure 20. Final manufactured test apparatus

Chapter 5: Final Design Verification

5.1 System Calibration

Arduino Script Inputs and Motor Control

The Arduino script mentioned in Section 4.5 was structured to control both the signal strength (from 1800 to 2000 microseconds) and the duration of the drive signal/command (from

.2-.65 milliseconds). A drive signal of 1800 provided enough power to drive the motor, while a drive signal of 2000 powered the motor at full speed. The Arduino script can be found in Appendix B.

Bats decelerate prior to impact with a catcher's helmet due to the batter's swing kinematics. To mimic this deceleration prior to impact, the team decided a swing angle of 270° for the mechanism to accelerate followed by bat deceleration towards impact. To do this, the test mechanism was marked at several angles along its counterclockwise path including 0°, 225°, and 270°. The bat was set at the 0° mark to begin a testing cycle and would accelerate until it reached the 225° mark. Then, the drive signal would have exceeded its preset duration input and would then continue its motion as the heavy friction and resistance provided by the gearbox and drivetrain slowed the angular velocity of the system. A 45° "coast zone" was allocated to allow for the bat to coast before impact at the final mark at 270°. The team gathered one set of data consisting of three test cycles where the bat began at -45°, allowing for a 315° bat path. This was done to yield slightly higher bat speeds at full power; the slightly elongated bat path allowed for the bat to accelerate longer before reaching the coast angle.

The strength of the signal dictated how quickly the bat would accelerate to the "coast zone" at 225°. The team experimented with several combinations of signal strengths and durations and attempted to balance the two inputs in order to yield different swing speeds while ensuring the bat begins decelerating near the coast angle of 225°.

Measuring Bat Speed

The team had originally planned to use an integrated gearbox encoder to measure the speed of the bat swing. Due to several complications, the team could not measure bat speed using the encoder. To measure bat speed the team used a slow motion camera (240hz) to capture video of each test. Using the video, the team observed the time it took for the tip of the bat to travel the final 45° of rotation. The time was then used to calculate average speed of the bat over the last 45° of rotation. Since the camera used during this process could only capture 240 frames per second, the team realized that the speed approximations have a degree of error. Only full frames could be measured, so bat-helmet collisions that occured between two frames proved difficult to accurately observe.

Upon experimenting with many combinations of Arduino script inputs, the team compiled a collection of approximate bat speeds (measured from 10-25 mph) corresponding to their Arduino script inputs. After this point, the team had considered that the mechanism was calibrated and could be operated in reference to an incremental index of predetermined inputs and bat speed outputs.

5.2 Testing Procedure

1. Ensure all connections in circuit are secure
2. Lined up headform with helmet with bat for specific impact
    a. Right side: Barrel of the bat lines up with halfway up the headform on the right cheek
    b. Back: Barrel of the bat lines up with halfway up the headform on the back of the head
3. Set headform at 270° marker
4. Set bat at starting position marker
5. Resdata logger which measures the Severity Index and peak g
6. Start video recorder
7. Upload Arduino script to Arduino
    a. Set strength of signal in microseconds
    b. Set delay to milliseconds corresponding to duration of drive signal
8. Power circuit by switching on circuit breaker switch
9. Run test
10. Record Severity Index and peak g displayed on the data logger
11. Repeat steps 1-10 for each test performed

5.3 Results

A headform with the weight of an average human's head, about 10 pounds, fixed to a linear track to allow acceleration from impact was used to collect data. The test procedure was used to collect Severity Index (SI) and peak g of the headform with and without helmets in different orientations. Table 6 displays the number of tests the team completed for each orientation with and without a helmet. The data can be seen in Appendix A. Figures 21-24 depict varying speed data for the four different system set-ups.

Table 6: Number of Tests Performed

Signal Strength	Duration	Average Speed (mph)	Helmet (Yes/No)	# of Tests (Right)	# of Tests (Back)
1875	650	10.23	No	4	5
			Yes	3	3
1915	310	13.75	No	2	2
			Yes	3	3
1925	300	17.00	No	2	2
			Yes	3	3
1975	225	19.26	No	2	2
			Yes	3	3
2000	250	21.00	No	0	2
			Yes	3	3
2000	300	24.50	No	0	2
			Yes	3	3

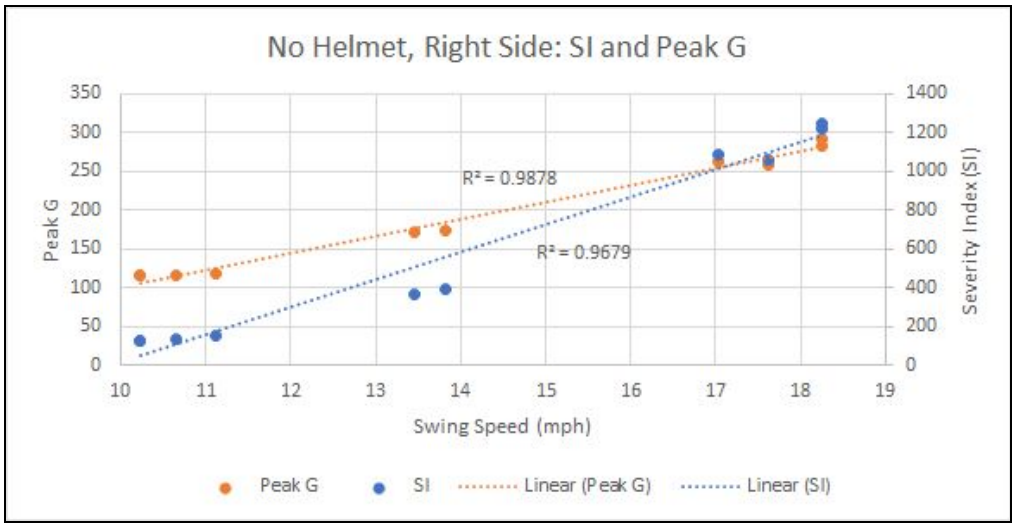

Figure 21: Graph for Right Side Collision Data with no Helmet

Figure 22: Graph for Right Side Collision Data with Helmet

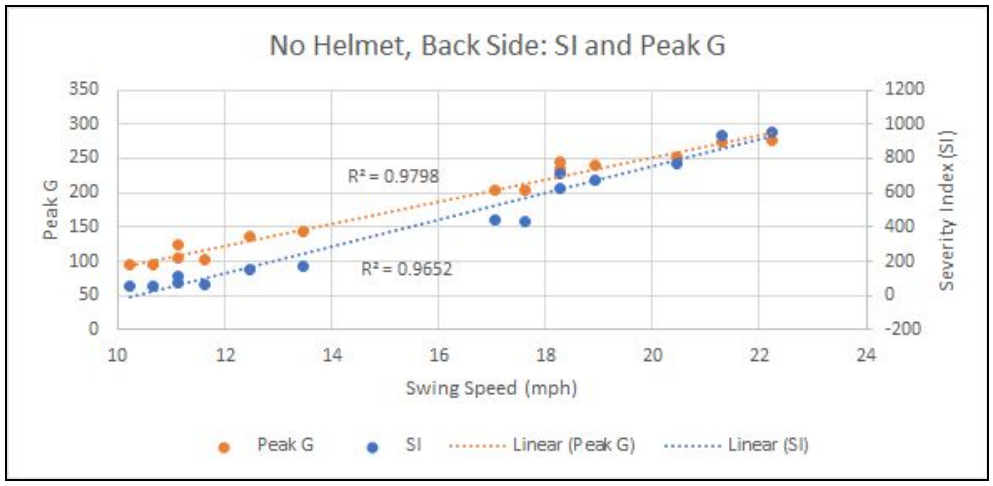

Figure 23: Graph for Back Collision Data with no Helmet

Figure 24: Graph for Back Collision Data with Helmet

Adding the helmet in the system greatly reduced the Severity Index and peak g readings of the collision. The data also closely represented a linear function between the swing speed and the Severity Index and peak g outputs. Table 7 depicts the slopes for the trendlines for the four graphs in Figures 21-24. These slopes measure the change in Severity Index and peak g over the measured bat speed at impact. The slopes for the non-helmet collisions were much higher than the non-helmet collisions.

Table 7: Treadline Slopes of Severity Index and Peak G values from experiments

	Right		Back	
	SI	Peak G	SI	Peak G
No Helmet	141.3	21.77	77.94	16.13
Helmet	1.027	1.945	2.976	3.954

Chapter 6: Final Design Validation

Table 8 demonstrates whether the final test system met design specifications expectations. In addition to meeting these criteria, the system as well as its individual components did not fail critically at any point during testing.

Table 8. Expectations of Test Apparatus Function Compared to Results

Criteria	Expectation	Met	Comment
Bat Speed	Match measure speed of 22 mph. Upper goal of 30 mph	Partial	Achieved peak impact speed of 25 mph.
Bat Path	Replicate Horizontal Bat Path	Yes	N/A
Size	Operates in normal work environment and easily transported	Yes	Transported fully assembled in a sedan
Operability	Easily and Safely Operated	Yes	Simple operation. Operator can be 12ft away.
Bat integrity	Prevent bat from breaking at impact or during acceleration	Yes	N/A
Budget	Remain within MQP budget constraints of $250 per a person	Yes	N/A
Repeatability	Test is easily repeatable.	Yes	Consistent output. Tests repeated quickly.
Cycle Limit	Bat is coasting at impact	Yes	N/A

Angular and Linear Acceleration Testing Differences

The highest reading for the team's experiment was a SI of 41 and a peak g value of 77 during a 25.5 mph collision on the back side of the headform with a helmet. The team performed a standard drop test to the specifications of the NOCSAE standard. The headform was dropped from 18 inches, resulting in an impact speed of 9.6 mph and readings of 240 and 82 for SI and peak p. However, the manufactured angular acceleration test is a more accurate representation of an actual bat swing compared to the NOCSAE required drop test. The results from each test were also drastically different as shown in Table 9. In order to match the momentum and energy of a linear drop test, the angular acceleration test must swing the bat at 162.74 mph and 30.56 mph, respectively. This shows that the linear acceleration test is testing to a higher SI than is possible to achieve in the angular acceleration apparatus.

Table 9. Speed, Momentum and Energy Comparisons Between Angular and Linear Acceleration Tests

	Angular Acceleration Test	NOCSAE Linear Acceleration Test
Speed (m/s)	4.911	4.233
Impact Momentum (Ns)	.4286	24.00
Impact Energy (J)	4.59	50.80

Viscoelastic Collision Modeling at the Brain

The primary outputs of the data logger are severity index and peak g. These can be used to understand the force, moment, and energy at impact. These values can be used to calculate the stress on the helmet and its varying layers of material until it reaches the skull and brain. The data collected is focused at the site of collision, which involves four viscoelastic materials including the bat, helmet shell, helmet lining, skull, and brain. Each of the materials has a spring and damping component that simultaneously disperse and absorb the applied forces, respectively. Figure 27 outlines a Voigt viscoelastic solid model of the system created at the site of collision.

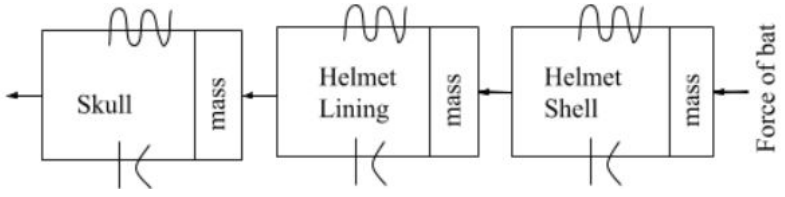

Figure 25. Lump Parameter Model of Stress on Brain from Bat Collision

Using a bulk-parameter model, the localized strain for each parameter can be calculated in parallel components using Equation 6 where ε is the strain, σ is the applied stress, E_1 is

Young's Modulus of the first parameter, E_2 is the modulus of the following parameter, η is the damping constant, and t is the time of applied stress (Pellicer 2004). The stress on the following parameter can be calculated using Equation 6 using the strain calculated from Equation 5. This process was repeated for each layer in the viscoelastic model until the output stress on the brain was obtained. The assumed and simplified stress on the brain as well as the brain's acceleration can be calculated to indicate risk levels of TBI and skull fracture.

$$\varepsilon(t) = \frac{\sigma_0}{E_2}\left[\left(\frac{E_1 + E_2}{E_1}\right) - e^{-\left(\frac{E_2}{\eta}\right)t}\right] \quad \text{Eq. 5}$$

$$\sigma(t) = \varepsilon_0 \frac{E_1 E_2}{E_1 + E_2}\left[1 + \frac{E_1}{E_2} e^{-\left(\frac{E_1 + E_2}{\eta}\right)t}\right] \quad \text{Eq. 6}$$

Using the collected data, the team was able to assess and predict the mechanical effects of the collision on the brain. One source shares that brain injury due to acceleration and impact on irregular surfaces has previously been shown to occur at maximum principal strain of 0.14-0.53 and a von Mises levels of stress of 5-17 kPa (Taylor 2018). Without a helmet, the initial stress applied on the skull would be 0.8 MPa, assuming a force impact of 2721 N over an area of 0.0034 m^2. Using the Voigt model outlined in Section 4.6 and the data collected by the team during testing, the maximum principal strain and von Mises stress values of 0.1×10^{-6} and 0.533 kPa, respectively. These calculations were performed using Young's Moduli and damping constants found in literature, and calculated strains at each layer. A time duration of impact was assumed to be 0.1 seconds. These values are outlined in Table 9.

Table 10. Values used in Equations 4 and 5 to calculate stress on each layer.

Layer	Modulus	Strain	Damping Constant (η)
Shell	2.3 GPa	3.6×10^{-4}	1.03 Ns/m^2
Foam	4.2 MPa	0.19	2.0 Ns/m^2
Skull	4.1 GPa	1.0×10^{-7}	0.053 Ns/m^2

Values without a helmet show much higher risk of skull fractures and traumatic brain injuries, whereas values with a helmet are well below the literature values of expected risk. Values including helmet protection are outlined in Table 10. However, this data is limited by current technology as it does not account for the multiple directions of both the principal and

shear stress. To accurately represent this collision, it is needed to reevaluate this in the future with more advanced technologies.

Table 11. Values calculated using Voigt Model of Viscoelastic Materials at 22 mph collision

Layer (impacted on)	Stress [Pa]	Strain
Shell	8002946	0.0003557
Foam	798803	0.1901912
Skull	818	0.0000002
Brain	533	0.0000001

The Voigt model explains conceptually how the force experienced at impact is decreased by the helmet to the values measured from the experiments. The stress applied to the head is significantly lower with the addition of a helmet compared to an impact without a helmet. With advanced technologies in which tests could define the force at impact, the team could compare values of the model and collected data.

Chapter 7: Discussion

Helmet Designs

Helmets are engineered to decrease stress concentration and fracture on the skull as well as stress and acceleration on the brain. After modeling the helmet layers, it is evident that each layer contributes to decreasing the translational energy and stress at each preceding layer. Future modifications to decrease stress values at the skull and brain layers could include a thicker layer of foam and shell materials as well as changing materials to those with a higher density. This would increase the impact energies within the helmet. Further understanding of material reactions to protect the brain, such as altering the geometry and stiffness of the materials, can also allow for controlled material compression rate and decrease risk of injury. Some current projects in advancing helmet structure technologies even include helmets with a suspension system and material upgrades, such as Rawlings' aerospace-grade carbon fiber/epoxy resin composite which is much stiffer and stronger than currently used ABS plastics (Rawlings, 2012).

Collected data showed higher SI results on the side of the headform without the helmet, but higher SI results on the back of the headform with the helmet. This is because the helmet is designed to be more protective at the side impact location due to the higher biological sensitivity at that location compared to the back of the head. Understanding the effects of altering helmet design structures is important in influencing the future of helmet design modifications and their standards.

Comparing Angular and Linear Acceleration Tests

The results of the team's angular acceleration tests produced SI and peak g values much lower than values yielded from data resulting in typical NOCSAE drop tests. Exploring the bare

headform data for both test types (Appendix A-3 & A-5) revealed that when the energy of the two types of tests were similar the measured SI for each test was also similar. Table 11 shows the similarity in the data between both test types. This supports that energy, not momentum, is the driving factor of SI and indicates that the drop test is a viable testing option for this type of one dimensional data collection. However, this also indicates that the test standards for the drop test produce much more energy than is possible to achieve with the angular test apparatus. Given that the angular test apparatus is designed to more closely imitate an actual back swing than the drop test, it is possible that the NOCSAE drop test standards could be changed in order to align with the designed testing model.

Table 12: Comparison between drop test and angular test bare headform data

Test Type	Data point 1		Data point 2		Slope (SI/J)
	Energy (J)	SI	Energy (J)	SI	
Drop Test	25	929	12.5	351	42.0
Angular Test	26.7	931	15.0	439	46.2

Discussions with industry experts indicated that at 1200 SI the skull is subjected to enough energy to possibly produce skull fractures. This lead the team to infer that these standards are primarily created to prevent against skull fracture over brain injuries such as concussions. The team believes that even though the standards test for a worst case scenario, updating the standard to test a more accurate angular acceleration would be beneficial for future development of catcher's masks with respect to concussion prevention.

The tests completed using angular acceleration appear to more accurately model more of the mechanical properties of impact. This led the team to inquire about current testing expectations and to investigate whether NOCSAE standards require high performance in tests that may not accurately model scenarios that occur during play. The graph in Figure 26 compares the NFL risk curve and data collected from Virginia Tech (VT) football players. The study recognized the major difference between the NFL data and the collected data from VT, and stated that the VT data was much more accurate as it has a much larger and unbiased data set to analyze. It is further explained that the NFL performed a biased study in search of head injury context as they performed a case control test. It was concluded that the NFL data was not properly normalized for head impact exposure (Funk, 2007).

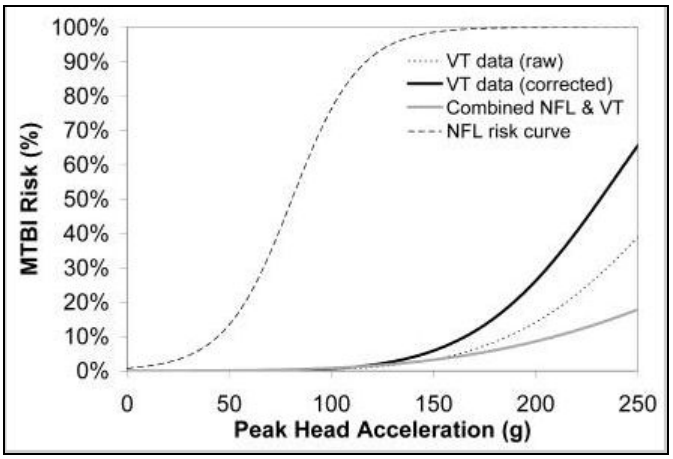

Figure 26. NFL data compared to Virginia Tech data comparing MTBI (moderate traumatic brain injury) and peak head acceleration

In regards angular test rig manufacturability, similar test rigs could be reproduced relatively easily and inexpensively. Most of the production time resulted from the design process rather than production.

Assumptions and Limitations

Although the performance and results of the angular acceleration test showed to be a better representation of a bat swing, there were still many assumptions that were made in order to make this project attainable. For example, the final design assumed a perfectly horizontal and circular bat path as well as several brain model simplifications. The headform used for testing was designed to collect data at the head's center of mass, so all data collected assumes the brain's location is there. The brain model and head injury predictions are based on a simplified brain model, as the brain is still too complex to fully understand and accurately model.

The data collected is also limited by the logging equipment used to calculate SI and peak g using accelerometers within the headform. This data-logging equipment was only calibrated within a linear SI calibration range of 300-1200. All of the "with helmet" data fell below this range, so this data is potentially inaccurate.

Finally, with current testing technologies, the team cannot calculate the force at impact, so it is difficult to accurately compare the Voigt model to collected data. Therefore, the model outlined in Section 4.6 is not supported by collected data. There are also limitations in understanding current traumatic brain injury factors and predictions as there are numerous biomechanical factors that are still not completely understood by experts.

Chapter 8: Conclusions and Recommendations

After collecting data from the experiments, it is evident that angular testing at previously measured backswing speeds yields much different results on head injury analysis compared to current drop tests standards. Current NOCSAE drop test standards may require higher helmet performance than what is expected during more realistic impacts. Helmet designs and experimentation procedures are constantly being improved to reduce risk of head injury, and understanding the differences between the linear drop test and the angular tests could help this process.

In future angular tests, it would be extremely beneficial to account for the two-dimensional and three-dimensional effects of the brain immediately after impact. The test used during this experiment had a 1D, linear acceleration output, measured by peak g and limited by the track the neck headform moves on. However, there are hybrid spring necks available to measure 3D acceleration of the brain. Neck stiffness also play a major role in how the head, and therefore the brain, react in these situations. This would further increase the understanding of brain injury by measuring directional angular accelerations (ω) to calculate the brain injury criteria equation shown in Equation 7 (Mueller), as well as further assess the validity of the drop test. Additionally, if allowed more time, the team would have tested products with varying amounts and materials of foam and shell combinations too see how SI and peak g readings were affected. For the future of these analyses, it would be important to use a test with angular acceleration in order to show the three-dimensional effects on the head from neck reactions.

$$: BRIC = \sqrt{\left(\frac{\omega_x}{66.25_{rad}}\right)^2 + \left(\frac{\omega_y}{56.45_{rad}}\right)^2 + \left(\frac{\omega_z}{42.87_{rad}}\right)^2} \quad \text{Eq. 7}$$

Given more time and funding the team would explore several design improvements for the test apparatus. The first change would be eliminating the design that allows slipping between the gearbox output shaft and the drive shaft. If this were eliminated, speed would be easier to control since there would be less during higher accelerations. Without slipping, an encoder could be used to measure speed. Although the final design included an encoder in the gearbox, this could not be used since the the drive shaft moved relative to the gearbox output shaft. The purpose of the slip design was to prevent backloading, but a design that features a clutch could have solved that problem while allowing for more controllable forward motion.

Another improvement would be including a more reliable method to measure speed of the bat for the current design. A key factor for this would be measuring the speed over a smaller interval than the last 45° of rotation to get a more accurate value for speed at impact. A laser gate would be a good solution for the current design, assuming it works well with a rotational system.

Finally, while the bat clamp sustained no damage, for future designs the team would recommend machining the clamp out of a stronger material. This would ensure clamp integrity at higher test speeds. Additionally, a design that allows the angle of the bat to change would allow for additional data to be collected on for various impact scenarios.

References

M.A. Fraser, D.R. Grooms, K.M. Guskiewicz, et al. “Ball-contact injuries in 11 National Collegiate Athletic Association Sports: the injury surveillance program, 2009–2010 through 2014–2015”. Journal of Athletic Training, 1062–6050–52.3.10. 2017. Available: https://doi.org/10.4085/1062-6050-52.3.10. [Accessed September 2018]

B.P. Boden, R. Tacchetti, F.O. Mueller. “Catastrophic Injuries in High School and College Baseball Players”. American Journal of Sports Medicine, 0363546503262161. 2004. Available: https://doi.org/10.1177/0363546503262161. [Accessed September 2018]

NOCSAE, “Standard Performance Specifications for Newly Manufactured Baseball/Softball Catcher’s Helmets with Faceguard”, NOCSAE DOC (ND) 024-18, pp. 1-17. Available: https://nocsae.org/wp-content/uploads/2018/05/1521574626ND02418MfrdBBCatchersHelmetsStd.Performance.pdf [Accessed September 2018]

T.B. Hoshizaki, S.E. Brien, “The Science and Design of Head Protection in Sport”, Neurosurgery, vol 55, no. 4, pp. 956-967, October 2004. Available: https://doi.org/10.1227/01.NEU.0000137275.50246.0B. [Accessed September 2018].

S. Gholampour, K. Hajirayat, A. Erfanian, A.R. Zali, E. Shakouri, “Investigating the Role of Helmet Layers in Reducing the Stress Applied During Head Injury Using FEM”, International Clinical Neuroscience Journal, vol. 4, no. 1, 2017. Available: https://doi.org/10.22037/icnj.v4i1.16691. [Accessed Febraury 2019].

X. Barksdale, “Catching Equipment that the Pros Wear”, Catching 101, Available: https://www.catching-101.com/catching-equipment-that-the-pros-wear/ [Accessed September 2018]

C. Robbins, 2017, July 18., “What Happens When You Have a Concussion?” [TedEd]. Available: https://ed.ted.com/lessons/what-happens-when-you-have-a-concussion-clifford-robbins#discussion. [Accessed October 2018].

N. Benac, “American Doctors Urge Medical Evaluations for All Concussed Athletes”, Canadian Medical Association Journal, 183, 1, E29-E30, Jan 2011. Available: https://doi.org/10.1503/cmaj.109-3739. [Accessed September 2018].

OpenStax: Anatomy and Physiology, Chapter 6: Bone Tissue and the Skeletal System [Textbook]. Available:https://tophat.com/marketplace/science-&-math/biology/textbooks/oer-openstax-anatomy-and-physiology-openstax-content/78/4156.[Accessed September 2018].

D.R. Namjoshi, et al., “Towards Clinical Management of Traumatic Brain Injury: A Review of Models and Mechanisms from a Biomechanical Perspective”, Disease Models & Mechanisms, 2013.

Available: https://openi.nlm.nih.gov/detailedresult?img=PMC3820257_DMM011320F2&req=4. [Accessed February 2019].

J. Newman, “Criteria for Head Injury and Helmet Standards”, NBEC Inc [Seminar], Medical College of Wisconsin, May 2005. Available: http://www.smf.org/docs/articles/hic/Newman_Snell_presentation.pdf. [Accessed November 2018].

M. Pellicer, J. Solà-Morales, “Analysis of a Viscoelastic Spring-Mass Model”, Journal of Mathematical Analysis and Applications, 294, pp. 687-689, 2004. Available: http://citeseerx.ist.psu.edu/viewdoc/download?doi=10.1.1.511.8822&rep=rep1&type=pdf. [Accessed October 2018].

Vex Robotics, VEX Robotics Motor Data - CIM Motor (217-2000) Available: https://motors.vex.com/vexpro-motors/cim-motor. [Accessed November 2018].

K. Taylor, “The Use of Decoupling Structures in Helmet Liers to Reduce Maximum Principal Brain Tissue Strain for Head Impacts”, Faculty of Health Sciences, University of Ottawa, 2018. Available: https://ruor.uottawa.ca/bitstream/10393/38536/1/Taylor_Karen_2018_Thesis.pdf. [Accessed December 2018].

Rawlings Sporting Goods Company, “MLB Players to Debut Rawlings S100 Pro Comp Batting Helmet”, April 2012. Available: https://www.prnewswire.com/news-releases/mlb-players-to-debut-new-rawlings-s100-pro-comp-batting-helmet-this-season-146991495.html. [Accessed February 2019].

J.R. Funk, S.M. Duma, S.J. Manoogian, S. Rowson, “Biomechanical Risk Estimates for Mild Traumatic Brain Injury”, Association for the Advancement of Automotive Medicine, vol. 51, pp. 343-361, 2007. Available: https://www.ncbi.nlm.nih.gov/pmc/articles/PMC3217524/. [Accessed February 2019]

B. Mueller, A. MacAlister, J. Nolan, D. Zuby, “Comparison of HIC and BrIC Head Injury Risk in IIHS Frontal Crash Tests to Real-World Head Injuries”, Insurance Institute for Highway Safety. Available: https://www-esv.nhtsa.dot.gov/proceedings/24/files/24ESV-000272.PDF. [Accessed February 2019].

Appendices

Appendix A: Testing Data

Hel?	Orientation	Test #	Strength	Duration	Frames	RPM	Speed (mph)	SI	Peak G	Force at Impact	Avg Force	Stress (MPa)
No	Right	1	1875	650	25	72.00	10.23	125	116	98.658	98.66	0.1019
No	Right	2	1875	650	25	72.00	10.23	128	115	97.808		
No	Right	1	1875	650	24	75.00	10.65	139	115	97.808		
No	Right	2	1875	650	23	78.26	11.11	153	118	100.359		
No	Right	1	1915	310	18.5	97.30	13.82	392	173	147.137	146.29	0.1511
No	Right	2	1915	310	19	94.74	13.45	369	171	145.436		
No	Right	1	1925	300	15	120.00	17.04	1089	262	222.831	221.56	0.2289
No	Right	2	1925	300	14.5	124.14	17.63	1060	259	220.280		
No	Right	1	1975	225	14	128.57	18.26	1247	292	248.346	244.09	0.2522
No	Right	2	1975	225	14	128.57	18.26	1217	282	239.841		

Figure A-1:Data for Right Side Collisions with no Helmet

Yes	Right	1	1875	650	25	72.00	10.23	0	10	8.505	9.07	0.0094
Yes	Right	2	1875	650	24	75.00	10.65	0	11	9.356		
Yes	Right	3	1875	650	24	75.00	10.65	0	11	9.356		
Yes	Right	1	1915	310	17	105.88	15.04	0	20	17.010	17.29	0.0179
Yes	Right	2	1915	310	18	100.00	14.20	0	23	19.562		
Yes	Right	3	1915	310	18	100.00	14.20	0	18	15.309		
Yes	Right	1	1925	300	14.5	124.14	17.63	0	24	20.412	20.98	0.0217
Yes	Right	2	1925	300	15.5	116.13	16.49	0	26	22.113		
Yes	Right	3	1925	300	15.5	116.13	16.49	0	24	20.412		
Yes	Right	2	1975	225	12.5	144.00	20.45	11	33	28.067	28.92	0.0299
Yes	Right	3	1975	225	13	138.46	19.66	10	34	28.917		
Yes	Right	5	1975	225	13	138.46	19.66	12	35	29.768		
Yes	Right	1	2000	250	11.5	156.52	22.23	12	38	32.319	26.08	0.0269
Yes	Right	2	2000	250	12.5	144.00	20.45	10	32	27.216		
Yes	Right	3	2000	250	12.5	144.00	20.45	0	22	18.711		
Yes	Right	1	2000	300	11	163.64	23.24	12	33	28.067	28.07	0.0290
Yes	Right	2	2000	300	11.5	156.52	22.23	10	30	25.515		
Yes	Right	3	2000	300	11.5	156.52	22.23	10	36	30.618		

Figure A-2:Data for Right Side Collisions with Helmet

No	Back	1	1875	650	23	78.26	11.11	111	123	104.612	88.62	0.0916
No	Back	2	1875	650	25	72.00	10.23	55	95	80.798		
No	Back	3	1875	650	24	75.00	10.65	52	95	80.798		
No	Back	1	1875	650	22	81.82	11.62	66	102	86.751		
No	Back	2	1875	650	23	78.26	11.11	74	106	90.153		
No	Back	1	1915	310	20.5	87.80	12.47	149	137	116.519	119.07	0.1230
No	Back	2	1915	310	19	94.74	13.45	168	143	121.622		
No	Back	1	1925	300	15	120.00	17.04	439	204	173.502	173.50	0.1792
No	Back	2	1925	300	14.5	124.14	17.63	432	204	173.502		
No	Back	1	1975	225	14	128.57	18.26	710	245	208.373	204.12	0.2109
No	Back	2	1975	225	14	128.57	18.26	630	235	199.868		
No	Back	1	2000	250	12.5	144.00	20.45	770	253	215.177	209.65	0.2166
No	Back	2	2000	250	13.5	133.33	18.94	669	240	204.120		
No	Back	1	2000	300	12	150.00	21.30	931	273	232.187	233.89	0.2416
No	Back	2	2000	300	11.5	156.52	22.23	956	277	235.589		

Figure A-3:Data for Back Side Collisions with no Helmet

Yes	Back	1	1875	650	21	85.71	12.17	6	31	26.366		
Yes	Back	2	1875	650	23	78.26	11.11	0	23	19.562	22.11	0.0228
Yes	Back	3	1875	650	23	78.26	11.11	0	24	20.412		
Yes	Back	1	1915	310	17	105.88	15.04	6	27	22.964		
Yes	Back	2	1915	310	18	100.00	14.20	7	28	23.814		
Yes	Back	3	1915	310	18	100.00	14.20	7	30	25.515		
Yes	Back	1	1925	300	15	120.00	17.04	17	48	40.824		
Yes	Back	2	1925	300	14.5	124.14	17.63	19	51	43.376	43.94	0.0454
Yes	Back	3	1925	300	14	128.57	18.26	25	56	47.628		
Yes	Back	1	1975	225	14	128.57	18.26	30	64	54.432		
Yes	Back	2	1975	225	14	128.57	18.26	25	60	51.030	54.72	0.0565
Yes	Back	3	1975	225	14	128.57	18.26	35	69	58.685		
Yes	Back	1	2000	250	11	163.64	23.24	31	64	54.432		
Yes	Back	2	2000	250	12	150.00	21.30	32	64	54.432	53.30	0.0551
Yes	Back	3	2000	250	12.5	144.00	20.45	29	60	51.030		
Yes	Back	1	2000	300	11	163.64	23.24	38	73	62.087	63.22	0.0653
Yes	Back	2	2000	300	10.5	171.43	24.35	39	73	62.087		
Yes	Back	3	2000	300	10	180.00	25.56	41	77	65.489		

Figure A-4:Data for Back Side Collisions with Helmet

Helmet?	Head Orientatior	Test Number	Speed (mph)	Severity Index	Peak G
No	Back	1	3.57	203	102
No	Back	2	3.55	202	105
No	Back	1	2.55	99	77
No	Back	2	2.54	103	77
No	Back	1	1.52	37	47
No	Back	2	1.55	35	47
No	Back	1	4.42	351	135
No	Back	2	4.47	348	135
No	Back	1	5.16	556	164
No	Back	2	5.18	560	165
No	Back	1	6.14	922	199
No	Back	2	6.11	928	200

Figure A-5: Drop test data for Back Side Collisions with no Helmet

Appendix B: Arduino Script

Victor_Code

```
#include <Servo.h>

Servo Victor; // Create Object "Victor"


void setup() {

 Victor.attach(5, 1000, 2000); // Attach signal line at pin 5, set minimum signal at 1000 microseconds, maximum at 2000 microseconds



}

void loop() {
 delay(5000);                  // 5 second delay between code upload and drive signal

 Victor.writeMicroseconds(2000); // Drive forward, in this case 2000 microseconds (full drive)
 delay(300);                   // For x miliseconds, in this case 300
 exit(0);


}
```